ROMANIAN JOURNAL OF INFORMATION SCIENCE AND TECHNOLOGY
Volume **18**, Number 4, 2015, 376–387

On the Necessary Verification of Fabrication Stages for SOI CMOS Humidity Sensors

Maria-Alexandra PAUN, Claudio FALCO, Florin UDREA

High Voltage Microelectronics and Sensors (HVMS) Group,
Department of Engineering, University of Cambridge
9 JJ Thomson Avenue, Cambridge, CB3 0FA, United Kingdom

E-mail: map65@cam.ac.uk

Abstract. A humidity sensor, which is part of an air quality sensor system, based on MWCNTs/MMA composite doped with KOH has been studied. A standard SOI CMOS process, with only one post-processing step for the membrane etching, was used to fabricate the sensor presented. In order to have a homogeneous distribution of the CNTs in the solution, the tip sonication method was employed. The current voltage and resistance voltage characteristics have been investigated, for different temperatures. Within the sensing layer of the proposed humidity sensor, the parabolic dependence of the resistance with the voltage applied has been proven for positive voltage values. The corresponding first and second order coefficients have been extracted.

Key words: humidity sensor; SOI CMOS technology, MMA; MWCNTs; KOH, resistive; relative humidity.

1. Introduction

The humidity sensing has largely become of interest over the last few decades, with applications in the fields of industry, various medical fields, in health assessment devices (such as incubators, sterilizers, respiratory equipment), in agriculture (soil moisture, moisture control in green houses and air quality control and improvement, dew detection in various agricultural crops) [1], in metrology, etc.

Various materials have been used in the realization of humidity sensors, such as ceramics, composites and polymers [2]. CMOS Humidity sensors have been used

recently for RFID application [3-4].The choice of a regular CMOS process to manufacture the humidity sensors offers the advantages of cost-effectiveness, robustness, and mass production [5-8]. Different types of humidity sensing instruments have been developed based on different work principles and diverse hygroscopic sensing materials [9–14].

In order to improve the performance of humidity sensors, one should master parameters like the sensitivity, linearity, power consumption, response time, hysteresis [15].

Recent works were devoted to characterize CMOS–MEMS Humidity sensors [16]. Previous works [2] have been focused on analyzing humidity sensors realized using Multi Wall Carbon Nanotubes (MECNTs) and poly (methyl methacrylate) (MWCNTs/PMMA) composite doped with Potassium hydroxide (KOH). Investigation into the necessary verification of the fabrications stages of such humidity sensors have been performed by the authors previously in [17].

This paper is intended to present a humidity sensor based on MWCNTs/MMA composite films, fabricated in a standard Silicon On Insulator (SOI) CMOS technology. The framework of the present research is to develop high sensitivity humidity sensors relying on carbon-based nanomaterials. More specifically, this work is intended to focus on MWCNTs with methyl methacrylate (MMA) composite thin film humidity sensor. The objective is to sense the relative humidity with an accuracy of $\pm$ 2% of full scale reading of 5% to 95% relative humidity around 300 K.

The humidity sensor presented in this work is part of an air quality sensing system. As the response characteristic of all the other sensors involved in the system depends on the humidity, a precise knowledge of this parameter is required to properly analyze the signal coming from the other sensing elements with high accuracy.

The paper is structured in four main sections. While Section 2 is intended to present the methods and materials used in the preparation of the humidity sensor, Section 3 summarizes the obtained results and discusses them. Finally the paper concludes in Section 4 and also mentions the future perspectives.

2. Methods and materials

2.1. Basic definitions

This section focuses on presenting the basic definitions of humidity metrics. Humidity is defined as the amount of water vapour in an atmosphere of air or other gases [18]. The following definitions and parameters are of interest, when talking about humidity in general.

Firstly, the Absolute Humidity (AH) is introduced as the ratio of the mass of water vapour in air to the volume of air and water vapour mixture [18]. The unit is grams per cubic meter and is expressed as following:

$$AH = \frac{m_w}{v}, \tag{1}$$

where m_w is the mass of the water vapour and v is the volume of air and the water

vapour mixture.

The Relative Humidity (Φ) [19] is defined as the ratio of the partial pressure of water vapor in the mixture e_w to the saturated vapor pressure of water e_w^* at a given temperature, and is given as a percentage.

$$\Phi = \frac{e_w}{e_w^*} \times 100. \tag{2}$$

The units of the pressures e_w and e_w^* are obviously Bar or KPa. We can note that due to the fact that the Relative Humidity depends on the temperature, it constitutes a relative measurement.

Thirdly, we talk about the Saturation Humidity (SH), which is the ratio of the mass of water vapour at saturation (m_{ws}) to the volume of air:

$$SH = \frac{m_{ws}}{v} \times 100. \tag{3}$$

Further on, we will briefly talk about the Dew and Frost points. On one hand, the Dew point is defined as a temperature, higher than 0℃, at which the water vapour content of the gas begins to condense into liquid water. We can say that the dew point is the temperature at which the saturation water vapour pressure is equal to the partial pressure of the water vapour (in an air atmosphere).

On the other hand, the Frost point is the temperature, smaller than 0℃, at which the water vapour in a gas condenses into ice. Dew and Frost points are parameters independent of temperature, and function of the pressure of the gas, therefore they provide absolute humidity measurements. The difference between the ambient temperature and the dew point temperature is a measure of the ambient relative humidity [20, 21].

2.2. Description of the solution

The solution, as described in the paper [2], contains 3 mL of MMA, 0.01 g of AIBN (in the form of a thin powder), 2 μL of KOH diluted in water at 50% (where 1 L = 1 ltr = 10^{-3} m^3, in SI base units). To the above, we have added CNTs in a concentration low enough to obtain a homogeneous dispersion without clusters (the exact amount is not fixed).

So far, it has been deposited on silicon for the first tries and on a chip with a top layer of silicon nitride and golden electrodes. It is to be noted that our solution contains KOH 50% rather than 10% used in the paper [2]. Due to the higher percentage of KOH in water solution used in our approach, we had to adjust the corresponding quantity to an amount of 2 μL. In this way, the handling of a smaller volume imposed for greater manipulation efforts.

The photographs in Figs. 1-2 (taken under microscope, at 5x magnification) depict the solutions we have used, with the clusters of CNTs, deposited on silicon substrate.

Figure 1 shows the first solution which contains shorter CNTs, whereas Fig. 2 presents the second solution, where we have used longer length CNTs.

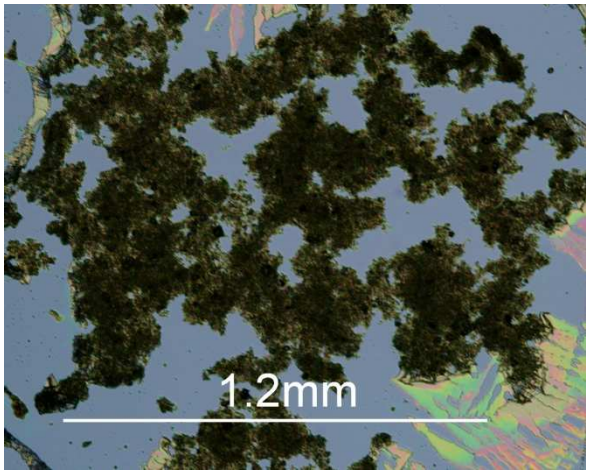

Fig. 1. Color photograph (5x) of the first solution.

Figure 2 emphasizes the second solution after sonication, where the darker spots correspond to agglomerations of CNTs. We can note that in Fig. 2, we have obtained a more homogeneous solution.

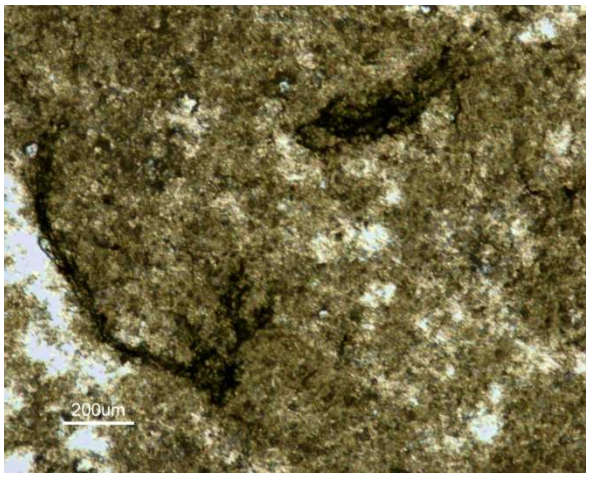

Fig. 2. Photograph (5x) of the second solution.

2.3. Preparation of the sensor

The humidity sensor was fabricated in a standard SOI CMOS process with only one post-processing step for the membrane formation using the deep reactive ion etching (DRIE).

We have used two types of chips in our approach, both with an area of approximately 1 mm^2. The first chip used, with the membrane diameter of 630 μm, has a

circular sensing area of diameter ∼250 μm, with electrodes of 5 μm width, spaced at 3 μm. For the second chip, the membrane and the sensing area coincide, with a square sensing area of ∼100 μm. In this case, the electrodes have both thickness and spacing of 2 μm, with the length as big as possible. For a quick overview, the Table 1 summarizes the dimensions of the system.

Table 1. System's dimensions

Chips	**Main dimensions**		
	Sensing Area Diameter **(μm)**	***Electrodes thickness*** **(μm)**	***Electrodes spacing*** **(μm)**
Chip 1	∼ 250	5	3
Chip 2	∼ 100	2	2

More specifically, the sensors were fabricated by tip-sonication and *in situ* synthesis on silicon substrate with a structure of gold interdigitated electrodes (IDE), as presented in Fig. 3. The photograph in Fig. 3 (taken under microscope, at 20x magnification) is a zoom of the sensing area of the first chip.

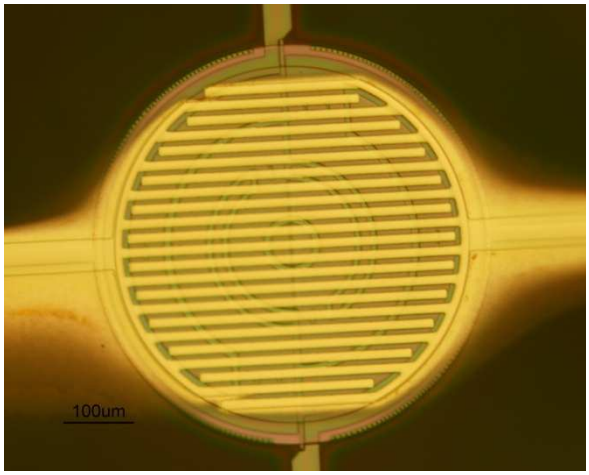

Fig. 3. Interdigitated Elecrodes (IDE) photograph (20x).

Once the solution presented above is ready (after adding in order MMA, KOH, AIBN and CNTs), it is tip-sonicated to have a homogeneous distribution of CNTs. We had to use the tip-sonication instead of bath-sonication, as it was more efficient in separating the CNTs. A small amount of solution is then sucked into a syringe and spilled out. The small amount of liquid left in the needle is squeezed out and dropped on the substrate. In this way, the amount of liquid is minimized and shows good dimension repeatability.

Once it is deposited, the solution is heated up at 343 K, to transform the MMA in PMMA [2]. This will create a matrix of water-sensible polymers and CNTs between the electrodes.

In Fig. 4, we can see the second attempt of the CNTs deposition onto the circular chip. In our second deposition attempt, we have used a different deposition technique – the DPN (Dip-pen nanolithography). At this stage, we were required to add terpineol to the solution, in order to avoid a quick evaporation of our solution in the air. In this case, we had a good control on position, dimension and CNTs density. In Fig. 4 (b), one could see the depositon after baking it in an oven, for 6 h at 343 K. After the baking process, most of the terpineol has been evaporated and the MMA polimerised in PMMA.

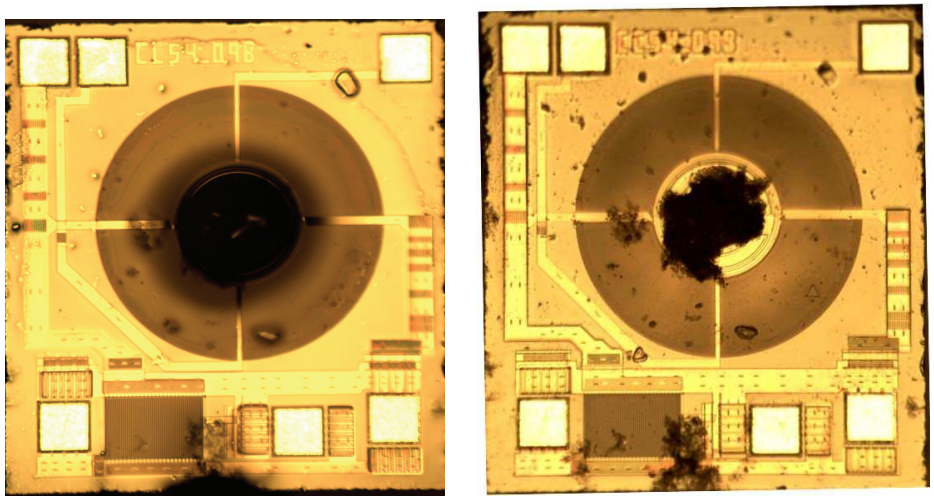

(a) **(b)**

Fig. 4. Second atempt of the deposition (a), deposition after baking (b).

We will now briefly describe the sensing mechanism of the humidity sensor. The matrix creates a conductive path between the golden electrodes, and has an electrical conductivity that depends on the amount of water absorbed or adsorbed. In the equilibrium condition, this depends on the amount of water in the air, and thus the humidity. Further measurements will prove if it depends on the relative or absolute humidity.

2.4. Quadratic dependence of the resistance with the temperature and applied voltage

A Taylor expansion of the $R = R(T)$ function, around the value T_0, has the form:

$$R(T) = R(T_0) + \frac{1}{1!}\frac{\partial R(T)}{\partial T}\bigg|_{T_0}(T - T_0) + \frac{1}{2!}\frac{\partial^2 R(T)}{\partial T^2}\bigg|_{T_0}(T - T_0)^2 + \\ + \sum_{n=3}^{\infty}\frac{1}{n!}\frac{\partial^n R(T)}{\partial T^n}\bigg|_{T_0}(T - T_0)^n \tag{4}$$

In the case in which

$$\sum_{n=3}^{\infty}\frac{1}{n!}\frac{\partial^n R(T)}{\partial T^n}\bigg|_{T_0}(T - T_0)^n = O[((T - T_0)^{n\geq 3})] \to 0, \tag{5}$$

we have after a simple computation and $R_0 = R(T_0)$, the simplified version of Eq. (4):

$$R(T) = R_0[1 + \alpha_T(T - T_0) + \beta_T(T - T_0)^2], \tag{6}$$

where

$$\alpha_T = \frac{1}{R_0}\frac{\partial R(T)}{\partial T}\bigg|_{T_0} \tag{7}$$

and

$$\beta_T = \frac{1}{2R_0}\frac{\partial^2 R(T)}{\partial T^2}\bigg|_{T_0} \tag{8}$$

are the "first and second (order) coefficients" of the temperature-related resistance.

Eq. (4) rewrites as a second order equation in $T - T_0$:

$$\beta_T(T - T_0)^2 + \alpha_T(T - T_0) - \frac{\Delta R}{R_0} = 0 \tag{9}$$

whose solution is:

$$T = T_0 + \frac{-\alpha_T + \sqrt{\alpha_T^2 + 4\beta_T\dfrac{\Delta R}{R_0}}}{2\beta_T}. \tag{10}$$

For a better understanding of the necessity of the temperature calculation using Eq. (10) in our system, we mention that the heater underneath is used to heat up the sensing layer at the optimum temperature, and the best way to have a feedback on this temperature is through the TCR.

Finally, in the case of our device, we have used the following numerical values for the temperature related coefficients, respectively $\alpha_T = 2.05 \times 10^{-3}\ K^{-1}$ and $\beta_T = 3 \times 10^{-7}\ K^{-2}$. Additionally, $T_0 = 298\ K$.

Analog, after the Taylor expansion of the function $R = R(V)$ around the value $V_0 = 0$ and $R_{01} = R(0)$, for the "first and second (order) coefficients" of the applied voltage-related resistance

$$\alpha_V = \frac{\partial R(V)}{\partial V}\bigg|_0, \quad \beta_V = \frac{1}{2}\frac{\partial^2 R(V)}{\partial V^2}\bigg|_0, \tag{11}$$

we find the simplified expression

$$R(V) = R_{01} + \alpha_V V + \beta_V V^2. \tag{12}$$

3. Results and Discussion

3.1. Investigation into the $I - V$ and $R - V$ characteristics

In order to obtain good quality humidity sensors, we have to start from microdevices functioning well and the parameters that need investigated are the I-V characteristic, resistance and the variation of the resistance with the voltage.

The following measurements on our sensor have been performed. We have biased the sensing layer with voltage from –3 V to 3 V and have recorded the current flowing through the sensing layer and computed the associated resistance. At the same time, we have recorded the voltage drop on the heater. We have repeated the above measurements for an array of different currents in the heater, namely 1mA, 4 mA, 7 mA, 10 mA, 13 mA and 16 mA. In this way, we had obtained information on the resistance variation.

As our humidity sensor is a resistive type, investigation in its resistance is important. The temperatures we have obtained, by measuring $\frac{\Delta R}{R_0}$ and using formula in Eq. (10), are the following: $T_1 = 298.0$ K, $T_2 = 303.8$ K, $T_3 = 312.9$ K, $T_4 = 326.9$ K, $T_5 = 345.0$ K and $T_6 = =371.3$ K. More specifically, the following graphs in Figs. 4-5 have been obtained, for the sensing layer within our humidity sensor.

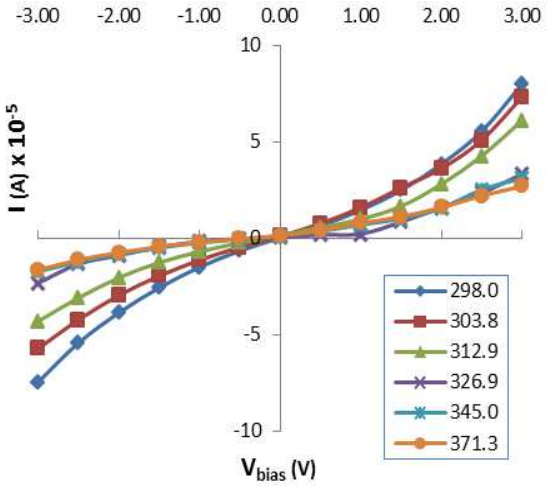

Fig. 5. Current-voltage characteristics for six temperatures.

The $I - V$ characteristics in Fig. 5 have been measured at six different temperatures. We can notice that these curves are dependent on the temperature. Also, it is worth observing that the current-voltage characteristics have a good symmetry with respect to (0, 0) point.

In line with the assumption in Eq. (12), we have identified the quadratic behavior of the resistance with the voltage. We have fitted the $R - V$ curves In Fig. 6 with second order polynomials, whose coefficients can be found in Table 2. We mention that the second order polynomial fittings have been performed on the positive voltage values, in the [0, 3 V] range.

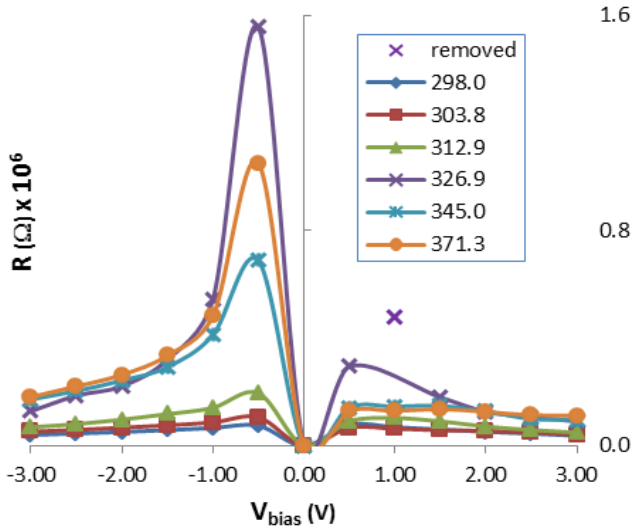

Fig. 6. $R - V$ characteristics for six temperatures.

Table 2. Fitting coefficients

T (°C)	T (K)	α_v	β_v	σ^2
25.0	298.0	1042	–19946	0.999
30.8	303.8	–1907	–3196	0.988
39.9	312.9	–7799	6573	0.917
53.9	326.9	25974	–17323	0.997*
72.0	345.0	–11291	17535	0.896
98.3	371.3	–6245	13766	0.838

*the fitting coefficients are obtained on the corresponding curve, after removing the 1 V point, by a statistical exclusion criterion.

3.2. Investigation into the humidity response

Further on, we were interested to verify if the proposed humidity sensor has a proper response to humidity. Figures 7–8 present the current and resistance behaviour

recorded over time, in the sensing layer, after subjecting the heater to a succession of various states when the heater was on, the heater off was and a relative humidity of 98% was induced. The data in Figures 7-8 is recorded for a maximum time of 600 s. We also mention at this point that the same biasing conditions have been used to obtain the experimental results in Figs. 7–8.

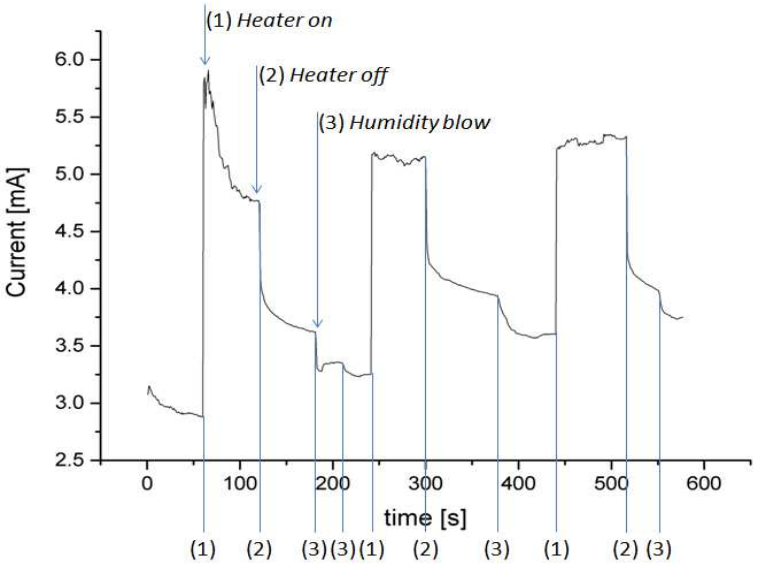

Fig. 7. Current behaviour over time, in the sensing layer.

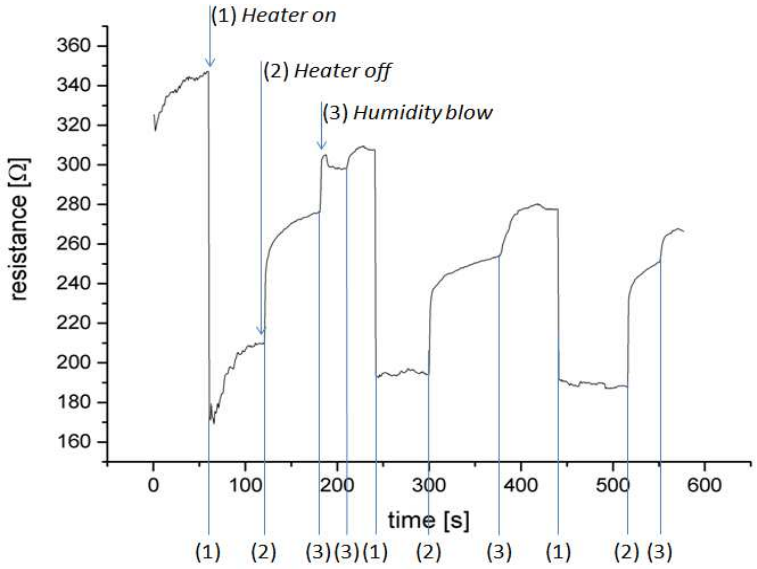

Fig. 8. Resistance behaviour over time, in the sensing layer.

To practically achieve this, the following steps have been followed. With respect to the biasing conditions, there was 1 V applied to the sensing layer and the heater was at 250℃when switched on. Moreover the heater was on in state (1) and off in state (2). Additionally, every time there was a blow on the chip ∼98% relative humidity was applied. This was done in state (3).

In Fig. 7, we can observe how the current changes between the switching on and off of the heater. Also, we can have an idea of the change of the current in the sensing layer, before and after the installation of humidity conditions. Additionally, in Fig. 8 the change in the resistance can be noticed for the same conditions (heater on, heater off, installation of humidity, and removal of the humidity conditions).

4. Conclusions and future perspectives

A humidity sensor based on MWCNTs/MMA composite films doped with KOH (diluted in water at 50%), fabricated in a standard SOI CMOS technology was studied. To have a better homogeneity of the CNTs, a tip-sonication step was performed in order to improve the quality of the deposition.

Regarding the humidity sensors proposed, the current-voltage and resistance-voltage characteristics have been investigated, through experimental measurements, for six different temperatures, using voltage biasing conditions in the range [–3 V, 3 V]. For the $R - V$ characteristic, second order polynomial fittings have been performed on the positive voltage values, in the [0, 3 V] range. The corresponding first and second order coefficients have been extracted.

In order to verify the good response of the proposed sensor to humidity, the changes in time of the current and resistance in the sensing layer have been recorded, for different conditions, such as when heater was in on and off states, also before and after the installation of humidity conditions.

Our immediate goal is to perform humidity tests on our sensors, for which we will be using a special chamber.

Acknowledgment. This work has been performed as part of the project "MSP - Multi Sensor Platform for Smart Building Management" (FP7-ICT-2013-10 Collaborative Project, No. 611887). Also, the first author, Maria-Alexandra Paun wishes to thank the Swiss National Science Foundation (SNSF) from Switzerland for the promotion and encouragement of the scientific research of young doctors, respectively by providing the funding for her advanced postdoctoral fellowship at Cambridge University, UK.

References

[1] CHEN Z., LU C., *Humidity Sensors: A review of materials and mechanisms*, Sensors Letters,**3**, 2005, pp. 274–295.

[2] SU P.-G., WANG C.-S., *In situ synthesized thin films of MWCNTs/PMMA doped with KOH as a resistive humidity sensor*, Sens. Actuators B, **124**, 2007, pp. 303–308.

[3] DENG F., HE, Y., ZHANG C., FENG, W., *A CMOS Humidity sensor for Passive RFID Sensing Applications*, Sensors, **14**, 2014, pp. 8728–8739.

[4] TAN Z., DAAMEN R., HUMBERT A., PONOMAREV Y. V., CHAE Y., PERTIJS M. A. P., *A 1.2 V 8.3 nJ CMOS Humidity Sensor for RFID Applications*, IEEE Journal Of Solid-State Circuits, **48** (10), 2013, pp. 2469–2477.

[5] NIZHNIK O., HIGUCHI K., MAENAKA K., *Self-calibrated Humidity Sensor in CMOS without post-processing*, Sensors, **12**, 2012, pp. 226–232.

[6] LAZARUS N., FEDDER G.K., *Designing a robust high speed CMOS-MEMS capacitive humidity sensor*, J. Micromech. Microeng. **22** 085021, 2012, pp. 1–7.

[7] AZERESO LEME C., BALTES H., *Multi-purpose interface for sensor systems fabricated by CMOS technology with post-processing*, Sens. Actuators A, **37–38**, pp. 77–81, 1993.

[8] QIU Y.Y., AZERESO LEME C., ALCACER L.R., FRANCA J.E., *A CMOS humidity sensor with on-chip calibration*, Sens. Actuators A, **92**, 2001, pp. 80–87.

[9] KASSAS A., *Humidity Sensitive Characteristics of Porous Li-Mg-Ti-O-F Ceramic Materials*, Am. J. Anal. Chem., **04**, 2013, pp. 83–89.

[10] ZHANG Y., YU K., JIANG D., ZHU Z.; GENG H., LUO L. ZINC, *Oxide Nanorod and Nanowire for Humidity Sensor*, Appl. Surf. Sci., **242**, 2005, pp. 212–217.

[11] KUANG Q., LAO C., WANG Z.L., XIE Z., ZHENG L., *High-Sensitivity Humidity Sensor Based on a Single SnO2 Nanowire*, J. Am. Chem. Soc., **129**, 2007, pp. 6070–6071.

[12] POKHREL S., JEYARAJ B., NAGARAJA K.S., *Humidity-Sensing Properties of ZnCr2O4-ZnO Composites*, Mater. Lett., **22–23**, 2003, pp. 3543–3548.

[13] CHEN Y.S., LI Y., YANG M.J., *Humidity Sensitive Properties of NaPSS/MWNTs Nanocomposites*, J. Mater. Sci., **40**, 2005, pp. 5037–5039.

[14] WANG K., QIAN X., ZHANG L., LI Y., LIU H., *Inorganic-Organic P-N Heterojunction Nanotree Arrays for a High-Sensitivity Diode Humidity Sensor*, ACS Appl. Mater. Interfaces, **5**, 2013, pp. 5825–5831.

[15] GU L., HUANG Q.-A., QIN M., *A novel capacitive-type humidity sensor using CMOS fabrication technology*, Sens. Actuators B, **99**, 2004, pp. 491–498.

[16] DENNIS J.-O., AHMED A-Y., KHIR M.-H., *Fabrication and Characterization of a CMOS-MEMS Humidity Sensor*, Sensors, **15**, 2015, pp. 16674–16687.

[17] FARAHANI H., WAGIRAN R., NIZAR HAMIDON M., *Humidity Sensors Principle, Mechanism and Fabrication Technologies: A Comprehensive Review*, Sensors, **14**, 2014, pp. 7881–7939.

[18] PAUN M.A, FALCO C., UDREA F., *SOI CMOS Humidity Sensor Based on MWCNTs/MMA Composite Films. On the Necessary Verification of Fabrication Stages*, Internationl Conference on Semiconductors, (CAS), Sinaia, Romania, October 12-14, 2015.

[19] PERRY R.H., GREEN D.W., *Perry's Chemical Engineers' Handbook* (7^{th} ed.), McGraw-Hill, 1999.

[20] *HIH Series Humidity Sensors*; Psychrometrics and Moisture, Reference and Application Data, Honeywell: Morristown, NJ, USA, pp. 145–147.

[21] FRADEN J., *Handbook of Modern Sensors*; Springer New York: New York, NY, 2010, pp. 445–459.